Journal of proteome research

Article

Cite This: J. Proteome Res. 2019, 18, 1237−1247

pubs.acs.org/jpr

# A Novel Truncated Form of Nephronectin Is Present in Small Extracellular Vesicles Isolated from 66cl4 Cells

Jimita Toraskar,[*,†,∥] Synnøve N. Magnussen,[⊥] Lars Hagen,[†,∥,#] Animesh Sharma,[†,#] Linh Hoang,[†,§] Geir Bjørkøy,[†,‡] Gunbjørg Svineng,[⊥] and Tonje S. Steigedal[†,∥]

[†]Department of Clinical and Molecular Medicine and [‡]Centre of Molecular Inflammation Research, Faculty of Medicine and Health Sciences, and [§]CMIC, Cellular and Molecular Imaging Core Facility, Norwegian University of Science and Technology, N-7491 Trondheim, Norway

[∥]Cancer Clinic, St. Olav's Hospital, Trondheim University Hospital, Trondheim, Norway

[⊥]Department of Medical Biology, Faculty of Health Sciences, UiT—The Arctic University of Norway, N-9037 Tromsø, Norway

[#]PROMEC, Proteomics and Modomics Experimental Core Facility, Norwegian University of Science and Technology, N-7030 Trondheim, Norway

*S* *Supporting Information*

**ABSTRACT:** Extracellular vesicles are emerging as biomarkers in breast cancer. Our recent report suggested that an intracellular granular staining pattern of the extracellular matrix protein nephronectin (NPNT) in breast tumor sections correlated with a poor prognosis. Furthermore, the results showed that NPNT is localized in extracellular vesicles derived from mouse breast cancer cells. In this study, we performed proteomic analysis that revealed that several proteins, including tumor-promoting molecules, are differentially expressed in the cargo of small extracellular vesicles (sEVs) derived from NPNT-expressing mouse breast cancer cells. We also identified three different forms of NPNT at 80, 60, and 20 kDa. We report that the native form of NPNT at 60 kDa becomes further glycosylated and is detected as the 80 kDa NPNT, which may be processed by matrix metalloproteinases to a shorter form of around 20 kDa, which has not previously been described. Although both 80 and 20 kDa NPNT are detected in sEVs derived from breast cancer cells, the 20 kDa form of NPNT is concentrated in sEVs. In summary, we show that a novel truncated form of NPNT is found in sEVs derived from breast cancer cells.

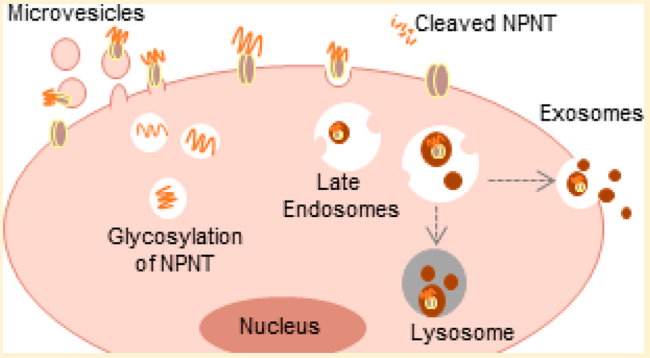


**KEYWORDS:** *breast cancer, nephronectin, small extracellular vesicles*

## 1. INTRODUCTION

Extracellular vesicles can be classified according to their size: exosomes (30−100 nm), microvesicles (100−1000 nm), apoptotic bodies (50 nm to 2 μm), and oncosomes (1−10 μm).[1] Microvesicles are bilipid-membrane vesicles originating from the plasma membrane,[2] initially disregarded as cellular debris but now recognized as biologically significant.[3,4] Extracellular proteins may enter into the intraluminal vesicles (ILVs) within multivesicular bodies (MVBs)[2] on inward budding of the plasma membrane. The invaginations of the limiting membrane of the MVBs further allow several intracellular proteins to enter into the ILVs.[5,6] The content of MVBs is either released as exosomes into the extracellular milieu or into the lysosomes for degradation.[7,8] The secreted exosomes may release their contents into a recipient cell by fusion or interact with the target cells via cell surface proteins.[9,10] Ultracentrifugation is regarded as the gold standard for exosome isolation.[11,12] However, it has been found that the pellet of vesicles obtained after spinning the supernatant of cells at 100 000*g* for 70 min contains a heterogeneous population of membrane vesicles, in addition to enriched exosomes.[13−16] Therefore, the preferred terminology for the isolated fraction is small extracellular vesicles (sEVs).[17]

The content of sEVs is not random;[18] rather, the cargo is cell and disease-type specific and may deliver discrete molecular messages that inflict a biological response.[19] sEVs are found to carry proteins,[20] lipids,[21] transposable genetic elements,[22] double-stranded DNA,[23] mitochondrial DNA,[24] and several types of RNAs.[25] Several extracellular matrix (ECM) proteins, such as collagens,[26] fibronectin,[27] vitronectin,[28] and nephronectin (NPNT), are found in sEVs.[29] NPNT has previously

**Received:** October 30, 2018
**Published:** February 1, 2019






DOI: 10.1021/acs.jproteome.8b00859
J. Proteome Res. 2019, 18, 1237−1247

been reported in isolated sEVs from human ductal saliva,[30] colorectal cancer cells,[31] and mouse breast cancer cells.[32,33]

Breast cancer is a heterogeneous disease and intercellular vesicular communication via sEVs may add to the complexity of the disease.[34] The sEVs released by breast cancer cells can survive in acidic and hypoxic environments and deliver procancerous proteins and transcripts to their target cells.[35] This induces a range of cellular responses within their target cells, to promote breast cancer development, progression, metastasis, and resistance toward therapy.[33,36−38] We have previously reported a correlation between intracellular granular NPNT staining pattern and decreased survival of breast cancer patients.[32] This granular staining pattern could represent NPNT-containing MVBs in tumor cells. Similar NPNT-positive granules have been observed in MMTV-PyMT tumor tissues and lung metastases from NPNT-expressing 66cl4 mouse breast cancer cells.[32] Furthermore, we have shown that NPNT is localized in sEVs isolated from 66cl4 cells overexpressing NPNT and that the localization of NPNT in sEVs is not dependent on the interaction of NPNT with the integrins.[32]

Here we examine the sEVs isolated from the supernatant of the 66cl4 cells overexpressing either wild-type NPNT (66cl4-NPNT) or NPNT mutated in the integrin binding sites (66cl4-NPNT-RGE and 66cl4-NPNT-RGEAIA). As a control, 66cl4 cells containing an empty vector (EV) were used (66cl4-EV). We report several proteins that are differentially packed in sEVs derived from 66cl4-NPNT cells compared to sEVs derived from 66cl4-EV cells. We have identified NPNT of 80, 60, and 20 kDa when analyzing whole-cell lysates of 66cl4-NPNT cells. The 80 kDa NPNT is the highly glycosylated form of the less glycosylated 60 kDa NPNT. We show here for the first time that a 20 kDa truncated form of NPNT is highly concentrated in sEVs.

## 2. MATERIALS AND METHODS

### 2.1. Cell Culture

The gene for NPNT was cloned and V5-tagged in the C-terminal, and the integrin-binding motifs were mutated and expressed in the mouse breast cancer cell line 66cl4, as previously described.[32] Four different variants of 66cl4 cell lines were created that harbored either an empty vector (66cl4-EV), expressed wild-type NPNT (66cl4-NPNT), NPNT where the RGD integrin-binding motif was mutated (66cl4-RGE), or where both the RGD and EIE-integrin binding motifs were mutated (66cl4-RGE-AIA).[32] All 66cl4 variants were cultured in (1×) minimum essential medium $\alpha$ (Thermo Fisher Scientific, Cat. No. 22561021), supplemented with 10% fetal calf serum, 1% (v/v) penicillin−streptomycin, and 1 M HEPES buffer (Thermo Fisher Scientific, Cat. No. 15630080).

### 2.2. Isolation of Extracellular Vesicles

Fetal calf serum (FCS) was depleted of extracellular vesicles using serial centrifugation and standard protocols.[32,39,40] The 66cl4 cell variants were grown in vesicular-free media for 3 days to reach approximately 80% confluency. The collected supernatant was centrifuged at 500$g$ for 10 min to remove cellular debris. The supernatant was carefully transferred and ultracentrifuged at 12 000$g$ for 20 min using a Beckman 70Ti rotor to isolate microvesicles (MVs) (pellet fraction 1). The supernatant was transferred to clean tubes and repelleted by ultracentrifugation at 100 000$g$ for 70 min, to isolate small extracellular vesicles (sEVs) (pellet fraction 2). PBS was used to wash both fractions of MVs and sEVs.

### 2.3. Preparation for Scanning Electron Microscopy (SEM)

Cultured cells grown on a Thermanox coverslip (Chemi-Teknik AS, Cat. No. 72280) were fixed with a solution of 2.5% glutaraldehyde (GA) (EM grade distillation purified, Chemi-Teknik AS, Cat. No. 16310) with 2% paraformaldehyde (PFA) (EMPROVE, VWR part of Avantor, Cat. No. 104005) in 0.1 M HEPES buffer for 2−4 h at room temperature. Cells were washed in 0.1 M HEPES buffer, subsequently dehydrated using increasing ethanol concentrations (25, 50, 70, 90, 2 × 100%) for 5 min each, followed by drying using hexamethyldisiloxane (HMDS) (50% and 2 × 100%, diluted in absolute ethanol) for 20 min each, and transferred to a desiccator to keep the samples dry. The dried samples were mounted on aluminum pins with double-sided carbon tape and sputter coated (Polaron) with 30 nm of gold/palladium. Samples were examined using a scanning electron microscope (Teneo SEM, Thermo Fisher Scientific) at a voltage of 5 kV.

### 2.4. Preparation for Transmission Electron Microscopy (TEM)

MVs and sEVs isolated and purified as described above were resuspended and fixed in cold 2% PFA in PBS. Droplets of MVs and sEVs were put on Formvar-carbon coated copper grids (200 mesh) for 5 min, fixed in 2.5% GA in 0.1 M Sorensen's phosphate buffer for 10 min, washed in reverse osmosis (RO) water, stained with 2% uranyl acetate (UA) in Milli-Q water for 4 min, and embedded in a solution of 2% UA and 3% poly(vinyl alcohol) (diluted 1:10) for 10 min. The excess liquid on the grids was then removed with filter paper (hardened) and air-dried. Grids were examined using a transmission electron microscope (JSM-1011 TEM, JEOL), at 100.000× magnification and a voltage of 80 kV. Images were captured with a Morada digital camera with iTEM software (BoRAS).

### 2.5. Uptake of Small Extracellular Vesicles

The pellet of sEVs was labeled with PKH26 (Sigma, MINI26), a dye taken up by the lipid membrane of sEVs. The 66cl4-EV cells supplemented with sEVs from 66cl4-EV and 66cl4-NPNT cells were fixed with 4% PFA for 4 h. Images were captured using a multichannel fluorescence imaging system (Thermo Fisher Scientific, EVOS).

### 2.6. Immunoblotting

Protein lysates were prepared using a mix of RIPA buffer (Thermo Fischer Scientific, Cat. No. 89901) and HALT phosphatase inhibitor single-use cocktail (Thermo Fischer Scientific, Cat. No. 78428). In some experiments, cells were pretreated with a final concentration of 100 nM of bafilomycin A1 (Sigma, Cat. No. SML1661) or 1× eBiocience protein transport inhibitor cocktail (PTI) (Invitrogen, Cat. No. 00-4980-93) for ≤6 h. To test the effect of GM6001 (Abcam, Cat. No. ab120845) on NPNT, cells were exposed to 10 $\mu$M of GM6001 for 24 h. To investigate the post-translational modification of NPNT, whole cell lysates were digested with different deglycosylation enzymes as per the manufacturer's protocol (New England Biolabs, Cat. Nos. P0704, P0733, and P0720). Samples equivalent to 30 $\mu$g each were loaded on a 10% Bis-Tris gel (Invitrogen). PVDF membranes were incubated with anti-V5 (CST, 13202) (1:1000) overnight at 4 °C. Unspecific binding was prevented by preincubating membrane in 5% BSA for 1 h at room temperature. Anti-GAPDH (Abcam, Cat. No. ab9484) (1:5000) and Anti-Alix (CST, Cat. No. 2171) were used as markers for whole cell lysate and sEVs, respectively. Pelleted fractions were checked for several other vesicular markers as previously reported.[32] HRP linked secondary antibody anti-mouse


DOI: 10.1021/acs.jproteome.8b00859
J. Proteome Res. 2019, 18, 1237−1247

(Dako, Cat. No. P0447) (1:5000) or HRP-linked anti-rabbit (Dako, Cat. No. P0399) (1:5000) were used. SuperSignal West femto substrate (Pierce, Cat. No. 34096) with an Odyssey Fc system (LI-COR Biosciences) was used for image analysis.

### 2.7. Immunoprecipitation and Gel Electrophoresis

V5-tagged NPNT was pulled down from 7 mg of whole cell lysates using 100 $\mu$L of anti-V5 (CST, Cat. No. 13202) (1:50) coated Dynabeads protein G (Thermo Fisher Scientific, Cat. No. 10003D) for 2 h at 4 °C. The beads were washed twice in PBS and proteins were eluted in LDS sample buffer (Invitrogen) for gel electrophoresis. 1D-PAGE of eluted proteins was performed in 10% NuPAGE Noves Bis-Tris gels using MOPS buffer. Proteins were visualized using SimplyBlue gel stain, and three bands (20, 60, and 80 kDa) were excised from the gel.

### 2.8. In Gel Digestion and Mass Spectrometry

SimplyBlue-stained protein bands corresponding to 80, 60, and 20 kDa, respectively, were manually cut out from the gel, and in-gel tryptic digestion was performed as previously described.[41] After desalting,[42] peptides were dried down in a SpeedVac centrifuge and resuspended in 0.1% formic acid. The peptides were analyzed on a LC−MS/MS platform consisting of an Easy-nLC 1000 UHPLC system (Thermo Fisher Scientific) interfaced with an LTQ-Orbitrap Elite hybrid mass spectrometer (Thermo Fisher Scientific) via a nanospray ESI ion source (Proxeon, Odense). Peptides were injected into a C-18 trap column (Acclaim PepMap100, 75 $\mu$m i.d. × 2 cm, C18, 3 $\mu$m, 100 Å, Thermo Fisher Scientific) and further separated on a C-18 analytical column (Acclaim PepMap100, 75 $\mu$m i.d. × 50 cm, C18, 2 $\mu$m, 100 Å, Thermo Fisher Scientific) using a multistep gradient with buffer A (0.1% formic acid) and buffer B ($CH_3CN$, 0.1% formic acid): From 0 to 6% B in 5 min, 6−12% B in 39 min, 12−20% B in 80 min, 20−28% B in 31 min, 28−40% B in 4 min, 40−100% B in 1 min, 100% B in 9 min, 100−0% B in 1 min, and 10 min with 100% A. The flow rate was 250 nL/min. Peptides eluted were analyzed on the LTQ-Orbitrap Elite hybrid mass spectrometer operating in positive ion and data-dependent acquisition mode using the following parameters: electrospray voltage 1.9 kV, CID fragmentation with normalized collision energy 35, and automatic gain control target value of 1E6 for Orbitrap MS and 1E3 for MS/MS scans. Each MS scan ($m/z$ 300−1600) was acquired at a resolution of 120 000 fwhm, followed by 20 MS/MS scans triggered for intensities above 500, at a maximum ion injection time of 200 ms for MS and 120 ms for MS/MS scans.

Proteins were quantified by processing MS data using Max Quant v 1.5.8.3.[43] Preview 2.3.5 (Protein Metrics Inc.) was used to inspect the raw data to determine optimal search criteria. The following search parameters were used: enzyme specified as trypsin with a maximum of two missed cleavages allowed; mass tolerance set to 20 ppm; oxidation of methionine and deamidation of asparagine and glutamine as dynamic post-translational modification, and carbamidomethylation of cysteine as a fixed modification. These were imported in MaxQuant, which uses $m/z$ and RT values to align each run against each other sample with 1 min window match-between-run function and 20 min overall sliding window using a clustering-based technique. These are further queried against the UniProtKB/Swiss-Prot database (Release April 2017 Mouse proteome with isoforms; 59684 sequences and MaxQuant's internal contaminants database) using Andromeda built into MaxQuant. Both protein and peptide identifications FDR were set to 1%; thus, only peptides with high confidence were used for final protein group identification. Peak abundances were extracted by integrating the area under the peak curve. Each protein group abundance was normalized by the total abundance of all identified peptides for each run and protein by calculated median summing all unique and razor peptide ion abundances for each protein using a label-free quantification algorithm[44] with minimum peptides ≥1. Protein group abundances were imported and analyzed using R software. Given the structure of the data, the statistical analysis was performed using a two-way analysis of variance (ANOVA) in order to consider the levels of variance at batch as well as test groups. Data were log 2-transformed before the analysis. Proteins were considered identified if they were quantified in at least 75% of the biological replicates. Noise with a standard deviation of 0.01 was added to compensate for the missing values followed by principal component analysis to find and remove the batch effect. Table S1 of the Supporting Information (SI) contains normalized log 2 intensity counts and corresponding values after the removal of the component. Perseus plugins[45] are used to carry out these steps. The latter values are only presented for those which have permutation based FDR < 5% with S0 of 0.1.[46] These are computed over $Z$-scored values with their medians, namely, the row representing the proteins intensities and the column representing the samples are shifted by the median of

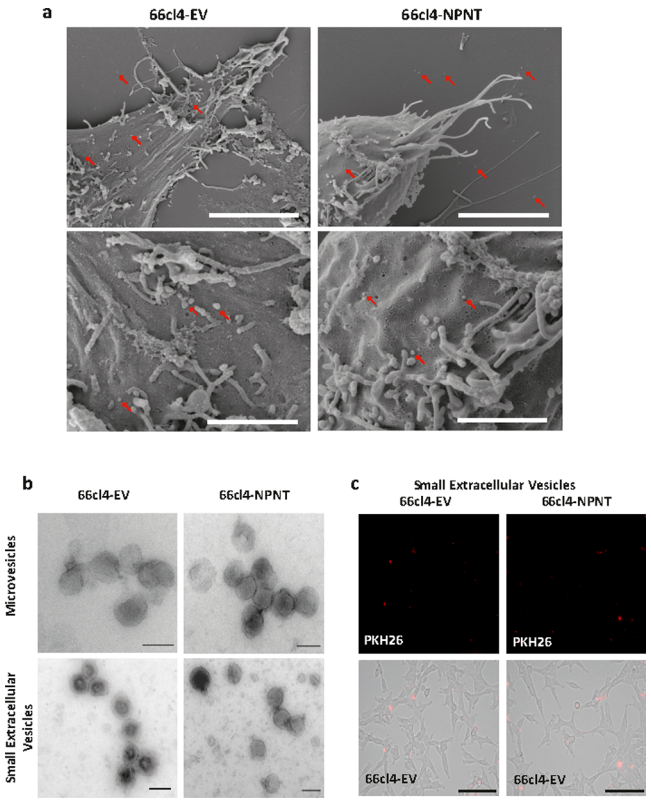


**Figure 1.** Overexpression of NPNT in 66cl4 cells does not affect the secretion or uptake of sEVs. (a) SEM of 66cl4-EV and 66cl4-NPNT cells cultured in medium free of serum vesicles for 24 h showed extracellular vesicles released by these cells. Red arrows point at potential extracellular vesicles. Scale bar, upper row 5 $\mu$m and lower row 2 $\mu$m. (b) Fractions of MVs and sEVs isolated from 66cl4-EV and 66cl4-NPNT cell lines were stained with uranyl acetate and viewed by electron microscopy. Scale bar, 100 nm. (c) 66cl4-EV cells were incubated with 40 $\mu$g of PKH26-stained sEVs derived from 66cl4-EV and 66cl4-NPNT cells and imaged after 4 h to check for internalization of exosomes. Scale bar, 100 $\mu$m.



DOI: 10.1021/acs.jproteome.8b00859
J. Proteome Res. 2019, 18, 1237−1247

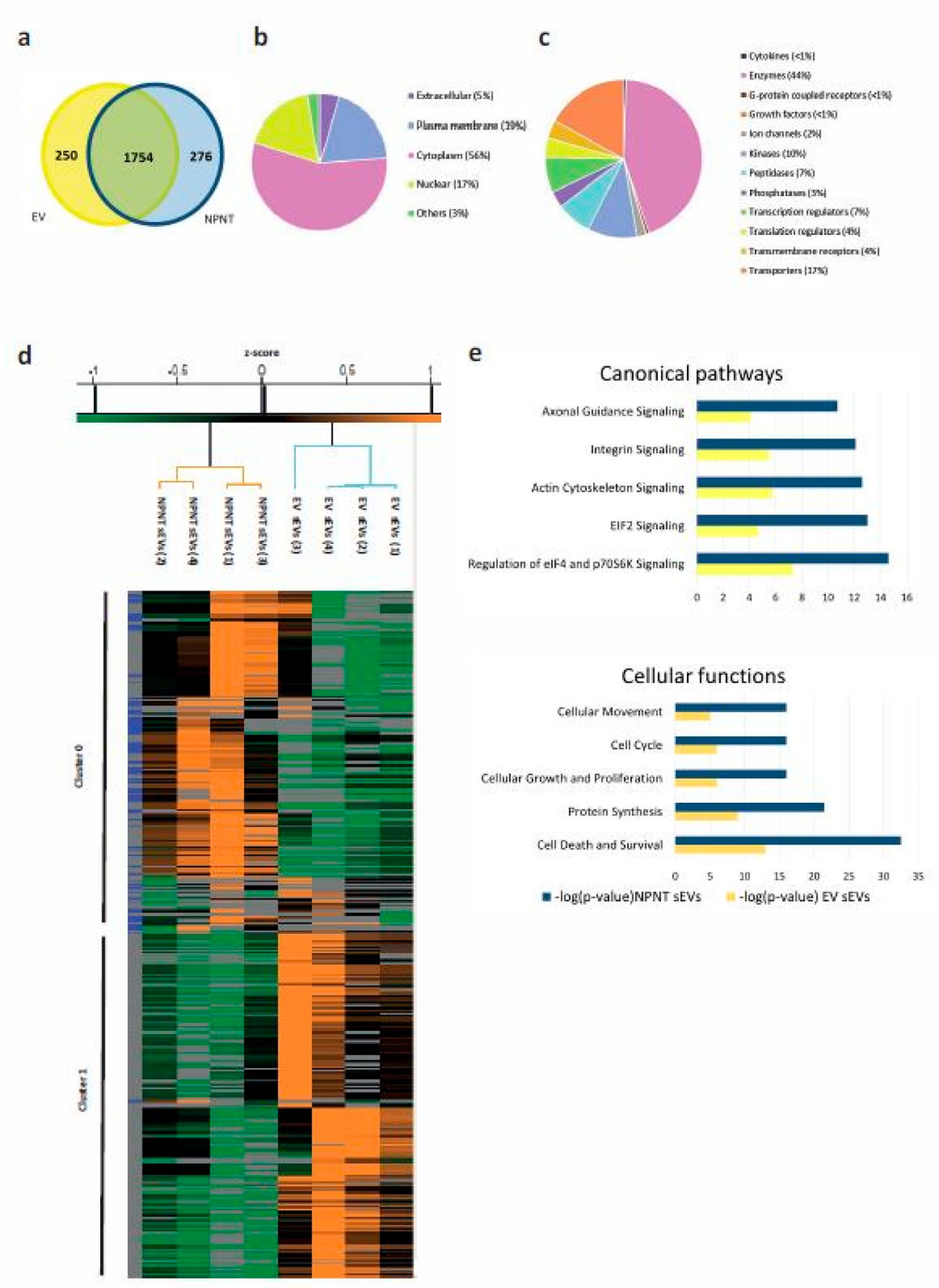


**Figure 2.** Overexpression of NPNT in 66cl4 cells alters the content of sEVs. (a) Venn diagram of proteins identified in sEVs isolated from 66cl4-EV and 66cl4-NPNT cells. A total 1754 proteins were identified to be common between the sEVs isolated from both of the cell lines. The numbers indicate that a certain protein was present in at least three out of four replicates. (b) Pie chart showing the distribution of 1754 common proteins based on their subcellular localization. (c) Pie chart showing the distribution of 1754 common proteins based on their molecular nature. (d) Heat map of proteins differentially expressed in sEVs derived from 66cl4-EV and 66cl4-NPNT cells, considering proteins from all four replicates. (e) Top canonical pathways and cellular functions predicted by IPA analyses using a list of proteins differentially expressed in sEVs derived from 66cl4-EV and 66cl4-NPNT cells.

the row and scaled by the standard deviation. Pearson's correlation coefficients were calculated in both dimensions over these values, which were further used for hierarchical clustering using an average linkage procedure (Figure 2d).

## 2.9. Ingenuity Pathway Analysis

In order to characterize the enrichment of functional category for selected protein groups (Table S1, SI, list of protein groups with permutation based FDR < 5% and S0 of 0.1), the



DOI: 10.1021/acs.jproteome.8b00859
J. Proteome Res. 2019, 18, 1237−1247

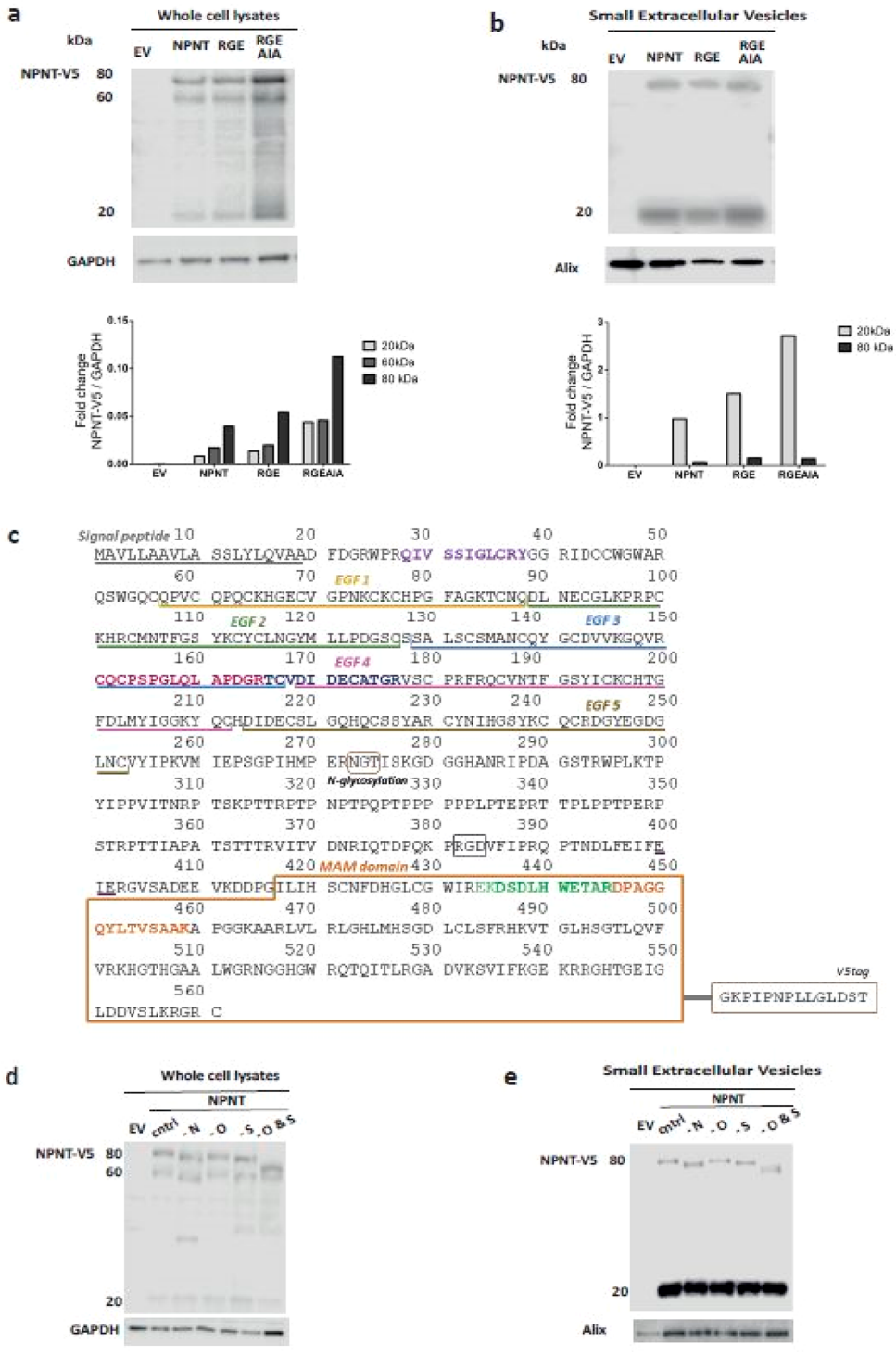


**Figure 3.** Truncated form of NPNT is concentrated in sEVs isolated from 66cl4-NPNT cells. (a) Immunoblotting for V5-tagged NPNT using whole cell lysates of 66cl4-EV, 66cl4-NPNT, 66cl4-NPNT-RGE, and 66cl4-NPNT-RGEAIA cells. (b) Immunoblotting for V5-tagged NPNT using lysates made from the sEVs isolated from supernatant of 66cl4-EV, 66cl4-NPNT, 66cl4-NPNT-RGE, and 66cl4-NPNT-RGEAIA cells. (c) Positional information on mouse NPNT sequences used for characterization of NPNT. Lysates made from whole cell (d) and small extracellular vesicles (e) of 66cl4 cells overexpressing NPNT were treated with different glycosylation enzymes and observed for reduction in the molecular size of NPNT. "-N" denotes removal of N-glycosylation by PNGase F treatment. "-O" denotes removal of O-glycosylation by O-glycosidase. "-S" symbolizes removal of the sialic acid cap. "-O&S" denotes removal of the sialic acid cap and O-glycosylation.

two broad clusters were mapped to the canonical pathways database of Ingenuity Pathway Analysis (IPA) (Qiagen).[47] The *p*-values based on Fisher's exact test over categorical distribution are corrected using Benjamini Hochberg procedure. They represent the statistical significance of the identified canonical functions, namely, the lower the *p*-value, the higher the proportion of identified proteins, overlapping with the particular canonical function.



DOI: 10.1021/acs.jproteome.8b00859
*J. Proteome Res.* 2019, 18, 1237−1247

## 3. RESULTS AND DISCUSSION

### 3.1. Overexpression of NPNT in 66cl4 Cells Does Not Affect the Secretion or Uptake of sEVs

To visualize the surface morphology and sEVs of 66cl4 cells, we utilized SEM. Several spherical particles in the nanometer range were observed on/around the cell surface (Figure 1a), suggesting the presence of extracellular vesicles. To confirm the presence of extracellular vesicles, we used differential ultracentrifugation and isolated extracellular vesicles from the supernatant of the 66cl4 cells, where pellet fraction 1 was collected upon spinning at 12 000*g* for 20 min and pellet fraction 2 was collected upon spinning at 100 000 g for 70 min. The isolated extracellular vesicles in the two pellets were characterized by TEM (Figure 1b), which is considered to be a standard tool for characterizing extracellular vesicles.[48] Double membrane vesicles were identified in both pelleted fractions 1 and 2. Fraction 1 displayed a homogeneous population of vesicles within the range 100−1000 nm, characteristic of MVs. Fraction 2 displayed vesicles within the range of 30−100 nm in diameter, characteristic of sEVs (Figure 1b). Overexpression of NPNT in 66cl4 cells did not alter the morphology nor the size of the MVs and sEVs, as observed by TEM analyses. The ability of sEVs to exert a functional effect mainly depends on their internalization and subsequent release of its content in recipient cells. We have previously detected NPNT protein in sEVs derived from 66cl4-NPNT cells.[32] To investigate if the presence or absence of NPNT in the sEVs affects its uptake, we treated sEVs derived from 66cl4-EV and 66cl4-NPNT cells with PKH26, a lypophilic dye, for 4 h prior to fixing and thorough washing of cells with PBS. PKH26-labeled vesicles were observed as red dots on and most likely within 66cl4-EV cells (Figure 1c), indicating that these vesicles are taken up or are bound to the surface of 66cl4-EV cells irrespective of their source and content.

### 3.2. Overexpression of NPNT in 66cl4 Cells Alters the Content of sEVs

To investigate the protein composition of sEVs upon NPNT overexpression, shotgun MS was performed on lysed sEVs derived from 66cl4-EV and 66cl4-NPNT cells. The Venn diagram (Figure 2a) shows the number of proteins identified in sEVs isolated from 66cl4-EV and 66cl4-NPNT cells. A total of 1754 proteins were identified to be common between the sEVs isolated from both cell lines. As expected, several well-known tumor and vesicular markers were detected in this common fraction between sEVs of both cell lines (Figure S1a, SI). A 62% similarity to the previously reported sEVs derived from parental 66cl4 cells was observed.[33] IPA analyses suggest that the majority of proteins in our data came from the cytoplasmic fraction of the cell (Figure 2b) and were enzymatic in nature (Figure 2c). NPNT was detected as one of the 276 proteins found only in sEVs derived from 66cl4-NPNT cells [Figure 2a and Table S1 (SI)]. Several kinases known for their role in tumor development, such as mTOR[49] and JAK,[50] were detected only in sEVs from 66cl4-NPNT cells (Table S1, SI). Ceruloplasmin, a known biomarker for breast cancer,[51] was only present in sEVs from 66cl4-NPNT cells. Two major clusters were identified when protein IDs passing a false discovery rate of 5% were clustered over *Z*-scores [Figure 2d and Table S1 (SI)]. NPNT is known to bind to different types of integrins,[52] and IPA analyses showed that several proteins identified in sEVs derived from 66cl4-NPNT cells are involved in integrin signaling pathways and are predicted to increase proliferation, cell survival, and organization of cytoskeleton/cytoplasm (Figure 2e). Several other studies have shown that a change in a single oncoprotein/oncogene can alter the contents of vesicular cargo and further incorporate tumor-promoting proteins in sEVs.[31,53−55] Taken together, the proteins enriched in sEVs derived from NPNT-expressing breast cancer cells might represent markers that are involved in mechanisms affecting breast cancer progression and metastasis.

### 3.3. Truncated Form of NPNT Is Concentrated in sEVs Isolated from 66cl4-NPNT Cells

The predicted molecular weight of mouse NPNT (561 amino acids) is 61 kDa. Our immunoblot analysis of 66cl4 cells overexpressing full length NPNT with a C-terminal V5-tag showed three bands of approximately 20, 60, and 80 kDa (Figure 3a). Interestingly, immunoblotting of lysed sEVs revealed only two bands, one at 20 and 80 kDa (Figure 3b). At the same time there was an increase in the relative amount of the 20 kDa NPNT in sEVs compared to the 80 kDa NPNT (Figure 3b). This could indicate that there is a selective sorting process involved in the vesicular packaging of NPNT. This phenomenon of the 20 kDa NPNT being concentrated was seen in both sEVs (Figure 3b) and MVs (Figure S1b, SI). Of note, we have observed that the quality of immunoblot is compromised upon freeze−thaw cycles of sEVs, and this might explain the difference in intensities in the 20 kDa bands in parts b and e of Figure 3.

To investigate whether the different apparent sizes of NPNT were due to post-translational modifications, we pulled-down NPNT from the whole cell lysates using V5 antibody and analyzed it by MS. Six unique NPNT peptide sequences were detected in the 80 kDa NPNT (Table 1), covering almost the full span of the protein (Figure 3c). This verifies that the 80 kDa NPNT is a full-length version of the protein. Four unique peptides matched the 60 kDa NPNT, including the first peptide (amino acids 28−37), indicating that the 60 kDa NPNT is most likely also a full-length version of the protein. One unique NPNT-derived peptide was detected in the 20 kDa NPNT (amino acid 446−459). This indicates that the 20 kDa NPNT is mostly harboring the MAM domain of the C-terminal part of the protein. Further, to identify whether post-translational modifications such as glycosylation contribute to differences between the three NPNT bands, whole cell lysates and sEVs were treated with PNGase F, O-glycosidase, or α2-3,6,8 neuraminidase. These enzymes remove N- and O-linked glycans with or without a sialic acid cap, thereby reducing the apparent molecular size of NPNT on immunoblots. Upon PNGase F treatment (-N), a reduction in the molecular size was observed for both the 60 and 80 kDa bands in whole cell lysates (Figure 3d) and for the 80 kDa NPNT of sEVs (Figure 3e). There was no shift in any

**Table 1. Characterization of 80, 60, and 20 kDa forms of NPNT[a]**

| NPNT sequence | length | start position | end position | 20 kDa | 60 kDa | 80 kDa |
|---|---|---|---|---|---|---|
| QIVSSIGLCR | 10 | 28 | 37 | – | √ | √ |
| CQCPSPGLQLAPDGR | 15 | 151 | 165 | – | – | √ |
| TCVDIDECATGR | 12 | 166 | 177 | – | √ | √ |
| EKDSDLHWETAR | 12 | 405 | 416 | – | √ | √ |
| DSDLHWETAR | 10 | 407 | 416 | – | √ | √ |
| DPAGGQYLTVSAAK | 14 | 417 | 430 | √ | – | √ |

[a]Whole cell lysates from 66cl4-NPNT cells were separated on the basis of their size by gel electrophoresis after immunoprecipitation with anti-V5-coated beads. In the eluted proteins, different NPNT tryptic peptides were detected in the 80, 60 and 20 kDa NPNT-V5 bands. The table represents results from three biological replicates.



DOI: 10.1021/acs.jproteome.8b00859
J. Proteome Res. 2019, 18, 1237−1247

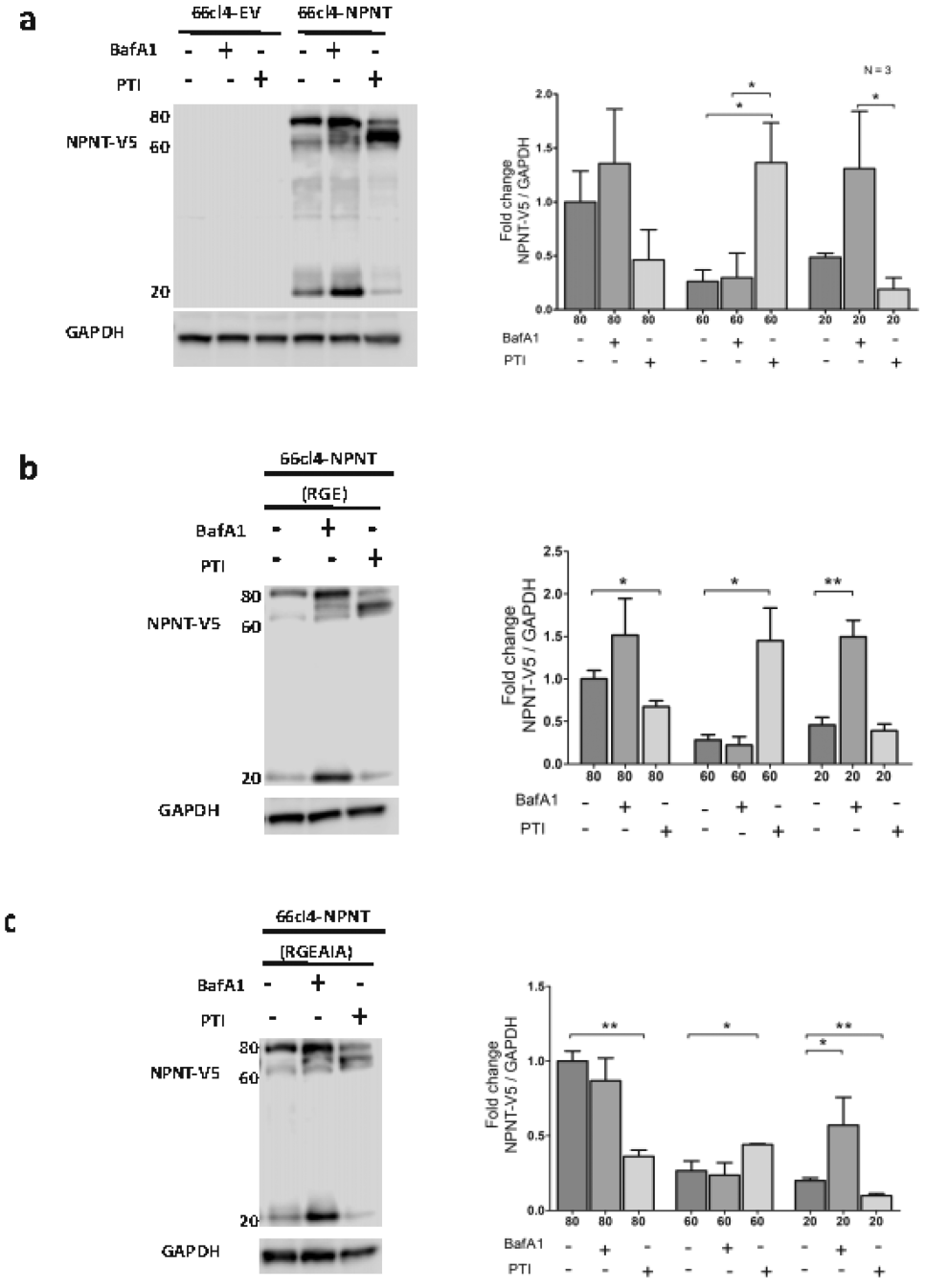


**Figure 4.** Intracellular protein trafficking controls the protein level of the truncated form of NPNT. (a) Immunoblotting for V5-tagged NPNT was used to detect differential expression of NPNT when 66cl4-overexpressing cells were exposed to 100 nM BafA1 or 1× PTI. (b) Immunoblotting was used to detect differential expression of V5-tagged NPNT in 66cl4-RGE cells after exposure to 100 nM BafA1 or 1X PTI for 6 h. (c) Immunoblotting for V5-tagged NPNT using whole cell lysates of 66cl4-RGE-AIA cells after exposure to 100 nM BafA1 or 1× PTI for 6 h. Results here are presented in terms of a fold change after normalizing with GAPDH. Quantification of optical density represents the mean of at least three independent experiments.

of the bands upon treatment with O-glycosidase (-O) alone. However, cotreatment with O-glycosidase and $\alpha$2-3,6,8 neuraminidase (-S) resulted in a major band shift in the 80 kDa NPNT for both cell and sEVs lysates. This suggests that the 80 kDa NPNT has O-glycosylation but with a sialic acid cap. A similar glycosylation pattern of NPNT secreted by osteoblasts has previously been reported.[56] A high degree of N- and O-glycosylation is predicted in the region between the EGF repeats and the MAM domains.[52] Aberrant glycosylation patterns of secreted glycoproteins are known to contribute in tumor development and progression.[57,58] It remains to be investigated whether the glycosylation pattern of NPNT would influence breast cancer progression. The glycosylation patterns are also crucial for sorting of proteins into extracellular vesicles.[59−61] Our results indicate that the 60 kDa band is far less glycosylated than the 80 kDa band, while the 20 kDa band is not glycosylated. The heavily glycosylated 80 kDa NPNT, containing both N- and O-glycosylations is recruited into sEVs (Figure 3e), while the less glycosylated 60 kDa NPNT is not detected in either sEVs or MVs. N-Glycosylations are mainly added when proteins transition through the endoplasmic reticulum,[62] while O-glycosylations are generally initiated in Golgi.[63]



DOI: 10.1021/acs.jproteome.8b00859
J. Proteome Res. 2019, 18, 1237−1247

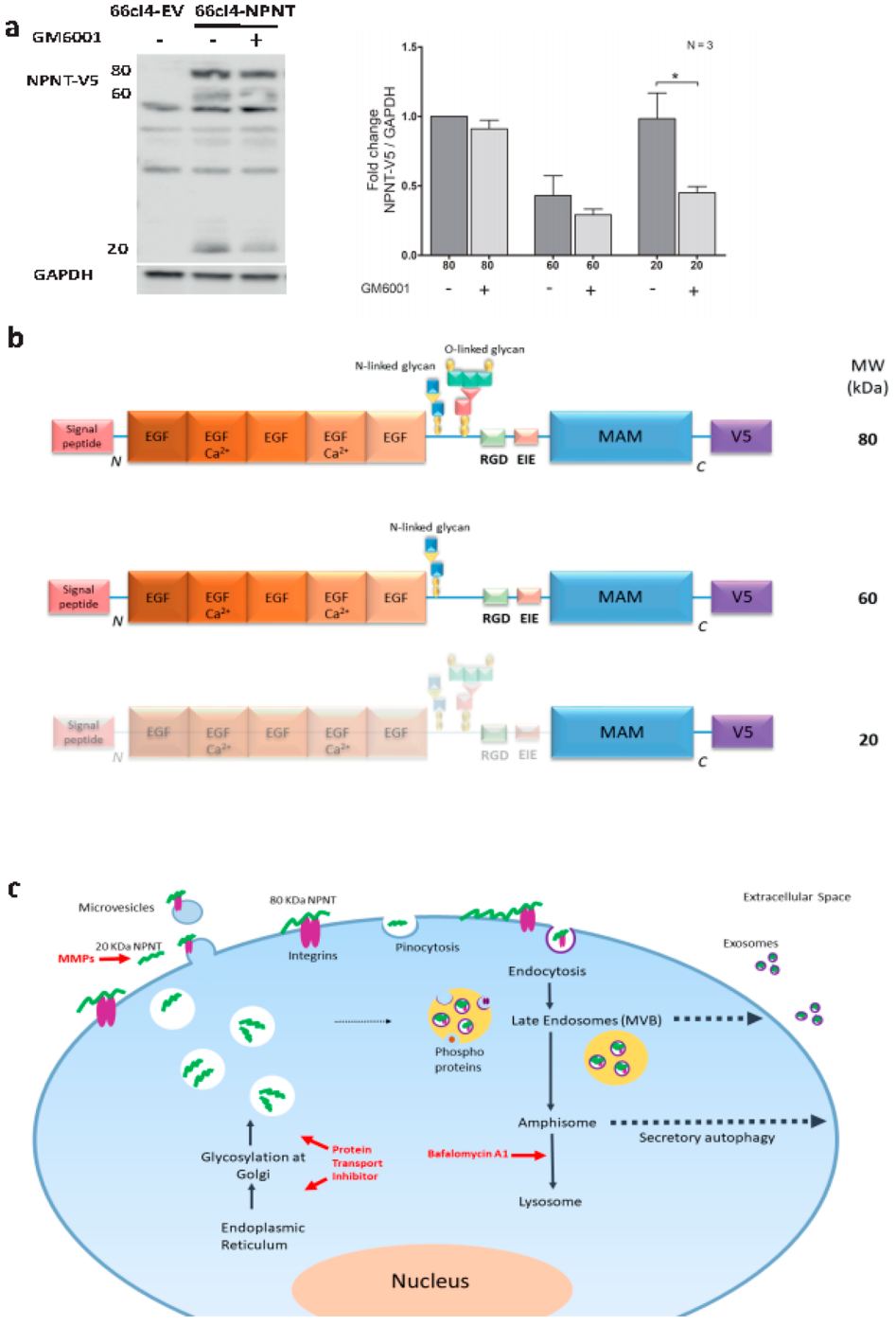


**Figure 5.** Matrix metalloproteinases are involved in proteolytic processing of full-length NPNT. (a) Immunoblotting for V5-tagged NPNT after exposure to 10 $\mu$M GM6001 for 24 h. Results here are presented in terms of a fold change after normalizing with GAPDH. Quantification of the optical density represents the mean of at least three independent experiments. (b) Illustration showing the structural differences in NPNT at 80, 60, and 20 kDa. The 80 kDa NPNT is the full-length protein having a putative signal peptide, the EGF repeats, glycosylation sites, integrin binding motifs, and the MAM domain. The 60 kDa NPNT is also a full-length protein but with fewer attached glycans, as opposed to the 80 kDa NPNT. The 20 kDa NPNT is the truncated form of NPNT harboring mainly the MAM domain and the C-terminal V5-tag. (c) Illustration showing the probable route of NPNT secretion, endocytosis, degradation, or selective sorting into extracellular vesicles. Upon glycosylation at the endoplasmic reticulum and Golgi, NPNT is secreted via secretory vesicles. The secreted NPNT probably interacts with cell surface receptors such as integrins or is cleaved by matrix metalloproteases (MMPs). The cleaved NPNT adhering to the cell surface could further be taken up and be released as exosomes or degraded by lysosomes, depending on the fate of multivesicular bodies.

### 3.4. Intracellular Protein Trafficking Controls the Protein Levels of the Truncated NPNT

The intracellular protein trafficking pathways are often manipulated in cancer cells, and a better understanding of this aspect is important for developing therapeutic interventions.[64] To investigate the intracellular NPNT trafficking, we employed a mixture of brefeldin A and monensin, to block transport from the endoplasmic reticulum to the Golgi apparatus, and bafilomycin A1 (BafA1), which inhibits degradation of endocytosed "cargo" by neutralizing the lysosomes[65] (Figure 5c). Hence, any



DOI: 10.1021/acs.jproteome.8b00859
J. Proteome Res. 2019, 18, 1237−1247

endocytosed protein, including NPNT, ends up being accumulated in the cytoplasm. 66cl4-EV and -NPNT cells were exposed to 100 nM BafA1, and whole cell lysates were harvested and analyzed by immunoblotting for the V5-tag. By inhibiting degradation of endocytosed proteins, there was a significant accumulation of the 20 kDa NPNT (Figure 4a) and a slight increase in 80 kDa NPNT. 66cl4-EV and -NPNT cells were exposed to 1× protein transport inhibitor cocktail (1× PTI), and whole cell lysates were harvested and analyzed by immunoblotting for the V5-tag. Inhibiting the secretion resulted in an accumulation of the 60 kDa band of NPNT, with a corresponding reduction of the 80 and 20 kDa bands (Figure 4a). Cells expressing the mutated forms of NPNT showed similar changes when exposed to PTI or BafA1 (Figure 4b,c). Taken together, these results indicate that the 60 kDa NPNT is not a secreted version of NPNT, but rather the "native" protein. This could also explain the limited amount of glycosylations present in the 60 kDa NPNT (Figure 3a) and its absence in the sEVs (Figure 3b). Both 80 and 20 kDa accumulate in the cytoplasm upon BafA1 treatment, indicating that they are both endocytosed from the extracellular milieu. The 80 kDa NPNT is most likely the secreted full-length version of NPNT, having both N- and sialic acid capped O-glycosylations.

### 3.5. Matrix Metalloproteinases (MMPs) Are Involved in Proteolytic Processing of Full-Length NPNT

Having identified the truncated form of NPNT, we further analyzed whether proteases such as MMPs are involved in this processing by utilizing GM6001, a broad-spectrum MMP inhibitor. 66cl4-NPNT cells were treated with 10 $\mu$M GM6001 for 24 h and whole cell lysates were analyzed by immunoblotting for the V5-tag. A significant reduction in the relative amounts of 20 kDa NPNT was observed (Figure 5a). We already know that the extracellularly located 80 kDa NPNT can be endocytosed by the cells. When MMP cleavage is inhibited, the amount of endocytosed 20 kDa NPNT is reduced. This indicates that the 20 kDa NPNT is a cleaved form of NPNT and that this cleavage is at least in part mediated by MMPs. MMPs can cleave proteins intracellularly and extracellularly.[66] Several metalloproteinases are also packed inside extracellular vesicles, capable of further altering the vesicular cargo by proteolytic processing.[67,68] Cleaved proteins packed in tumor-derived extracellular vesicles are reported to be biologically active.[55,69] Further investigation is needed to identify if the cleaved NPNT packed in sEVs has a biological significance. Our study on NPNT trafficking in 66cl4 cells is the first to report a truncated form of NPNT at 20 kDa, mainly harboring the MAM domain part of the protein (Figure 5b). The exact MMP cleavage site and the identity of the MMPs capable of cleaving NPNT remain to be determined.

Though there are several challenges while analyzing the vesicular proteome using MS, the composition of sEVs derived from 66cl4-NPNT cells helps us to picture the molecular fingerprint of exosomes in cells with high NPNT levels. Results from the current study are summarized in Figure 5c and show that the native form of NPNT gets glycosylated and modified at the endoplasmic reticulum and Golgi and that the secreted full-length NPNT (80 kDa) probably gets cleaved by MMPs. Both the highly glycosylated NPNT (80 kDa) and the truncated form of NPNT (20 kDa) are perhaps endocytosed/pinocytosed and get incorporated into the ILVs within a MVB. These ILVs packed with NPNT inside a MVB can either be released as exosomes or be degraded by lysosomes.

## ■ ASSOCIATED CONTENT

### Supporting Information

The Supporting Information is available free of charge on the ACS Publications website at DOI: 10.1021/acs.jproteome.8b00859.

Table S1 in spreadsheet format (XLSX)

Figure S1, a list of well-known tumor and vesicular markers detected in sEVs isolated from 66cl4-EV and 66cl4-NPNT cells and mmunoblotting for V5-tagged NPNT using lysates made from the microvesicles isolated from the supernatant of 66cl4-EV and 66cl4-NPNT cells, and Table S1, a list of proteins identified in sEVs isolated from 66cl4-EV and 66cl4-NPNT cells (PDF)

## ■ AUTHOR INFORMATION


### Corresponding Author

*E-mail: jimita.toraskar@ntnu.no. Mobile phone:+47-99673377.

### ORCID

Jimita Toraskar: 0000-0002-5404-061X

Gunbjørg Svineng: 0000-0002-5947-5647


### Notes

The authors declare no competing financial interest.

The mass spectrometry proteomics data have been deposited to the ProteomeXchange Consortium via the PRIDE partner repository with the dataset identifier PXD010999.[70,71]

## ■ ACKNOWLEDGMENTS

The study received funding from the Central Norway Regional Health Authority (Project number: 46077600), North Norwegian Regional Health Authorities (Project number SFP1232-15), The Erna and Olav Aakre Foundation for Cancer Research, The Blix Family Fund for Medical Research, CMIC, and UiT. Dr. Fred Miller kindly provided 66cl4 and 4T1 mouse cell lines. Data storage and handling is supported under the Norstore/Notur project NN9036K and PRIDE. We express our gratitude to Dr. Naoko Morimura for the pcDNA3-POEM-Fc vector and Dr. Peter McCourt for linguistic revision. We thank Hector Peinado, Lucia Robado de Lope, and Marta Hergueta-Redondo for collaboration regarding exosome isolation protocols.

## ■ REFERENCES


(1) The International Society for Extracellular Vesicles. www.isev.org.

(2) van der Pol, E.; Boing, A. N.; Harrison, P.; Sturk, A.; Nieuwland, R. Classification, functions, and clinical relevance of extracellular vesicles. *Pharmacol. Rev.* **2012**, *64* (3), 676−705.

(3) Pucci, F.; Pittet, M. J. Molecular pathways: tumor-derived microvesicles and their interactions with immune cells in vivo. *Clin. Cancer Res.* **2013**, *19* (10), 2598−604.

(4) Jansen, F.; Yang, X.; Proebsting, S.; Hoelscher, M.; Przybilla, D.; Baumann, K.; Schmitz, T.; Dolf, A.; Endl, E.; Franklin, B. S.; Sinning, J. M.; Vasa-Nicotera, M.; Nickenig, G.; Werner, N. MicroRNA expression in circulating microvesicles predicts cardiovascular events in patients with coronary artery disease. *J. Am. Heart Assoc.* **2014**, *3* (6), e001249.

(5) Palmulli, R.; van Niel, G. To be or not to be··· secreted as exosomes, a balance finely tuned by the mechanisms of biogenesis. *Essays Biochem.* **2018**, *62* (2), 177−191.

(6) Thery, C. Exosomes: secreted vesicles and intercellular communications. *F1000 Biol. Rep.* **2011**, *3*, 15.

(7) Pan, B. T.; Teng, K.; Wu, C.; Adam, M.; Johnstone, R. M. Electron microscopic evidence for externalization of the transferrin receptor in vesicular form in sheep reticulocytes. *J. Cell Biol.* **1985**, *101* (3), 942−8.




DOI: 10.1021/acs.jproteome.8b00859
*J. Proteome Res.* 2019, 18, 1237−1247

(8) Harding, C.; Heuser, J.; Stahl, P. Endocytosis and intracellular processing of transferrin and colloidal gold-transferrin in rat reticulocytes: demonstration of a pathway for receptor shedding. *Eur. J. Cell Biol.* **1984**, *35* (2), 256−63.
(9) Montecalvo, A.; Larregina, A. T.; Shufesky, W. J.; Stolz, D. B.; Sullivan, M. L.; Karlsson, J. M.; Baty, C. J.; Gibson, G. A.; Erdos, G.; Wang, Z.; Milosevic, J.; Tkacheva, O. A.; Divito, S. J.; Jordan, R.; Lyons-Weiler, J.; Watkins, S. C.; Morelli, A. E. Mechanism of transfer of functional microRNAs between mouse dendritic cells via exosomes. *Blood* **2012**, *119* (3), 756−66.
(10) Costa Verdera, H.; Gitz-Francois, J. J.; Schiffelers, R. M.; Vader, P. Cellular uptake of extracellular vesicles is mediated by clathrin-independent endocytosis and macropinocytosis. *J. Controlled Release* **2017**, *266*, 100−108.
(11) Li, P.; Kaslan, M.; Lee, S. H.; Yao, J.; Gao, Z. Progress in Exosome Isolation Techniques. *Theranostics* **2017**, *7* (3), 789−804.
(12) Thery, C.; Amigorena, S.; Raposo, G.; Clayton, A. Isolation and characterization of exosomes from cell culture supernatants and biological fluids. *Current Protocols in Cell Biology*; Wiley, 2006; Chapter 3, Unit 3.22.
(13) Bobrie, A.; Colombo, M.; Krumeich, S.; Raposo, G.; Thery, C. Diverse subpopulations of vesicles secreted by different intracellular mechanisms are present in exosome preparations obtained by differential ultracentrifugation. *J. Extracell. Vesicles* **2012**, *1*, 18397.
(14) Willms, E.; Johansson, H. J.; Mager, I.; Lee, Y.; Blomberg, K. E.; Sadik, M.; Alaarg, A.; Smith, C. I.; Lehtio, J.; El Andaloussi, S.; Wood, M. J.; Vader, P. Cells release subpopulations of exosomes with distinct molecular and biological properties. *Sci. Rep.* **2016**, *6*, 22519.
(15) Kowal, J.; Arras, G.; Colombo, M.; Jouve, M.; Morath, J. P.; Primdal-Bengtson, B.; Dingli, F.; Loew, D.; Tkach, M.; Thery, C. Proteomic comparison defines novel markers to characterize heterogeneous populations of extracellular vesicle subtypes. *Proc. Natl. Acad. Sci. U. S. A.* **2016**, *113* (8), E968−77.
(16) Zhang, H.; Freitas, D.; Kim, H. S.; Fabijanic, K.; Li, Z.; Chen, H.; Mark, M. T.; Molina, H.; Martin, A. B.; Bojmar, L.; Fang, J.; Rampersaud, S.; Hoshino, A.; Matei, I.; Kenific, C. M.; Nakajima, M.; Mutvei, A. P.; Sansone, P.; Buehring, W.; Wang, H.; Jimenez, J. P.; Cohen-Gould, L.; Paknejad, N.; Brendel, M.; Manova-Todorova, K.; Magalhães, A.; Ferreira, J. A.; Osorio, H.; Silva, A. M.; Massey, A.; Cubillos-Ruiz, J. R.; Galletti, G.; Giannakakou, P.; Cuervo, A. M.; Blenis, J.; Schwartz, R.; Brady, M. S.; Peinado, H.; Bromberg, J.; Matsui, H.; Reis, C. A.; Lyden, D. Identification of distinct nanoparticles and subsets of extracellular vesicles by asymmetric flow field-flow fractionation. *Nat. Cell Biol.* **2018**, *20* (3), 332−343.
(17) Hessvik, N. P.; Llorente, A. Current knowledge on exosome biogenesis and release. *Cell. Mol. Life Sci.* **2018**, *75* (2), 193−208.
(18) Edgar, J. R. Q&A: What are exosomes, exactly? *BMC Biol.* **2016**, *14*, 46.
(19) Gangoda, L.; Boukouris, S.; Liem, M.; Kalra, H.; Mathivanan, S. Extracellular vesicles including exosomes are mediators of signal transduction: are they protective or pathogenic? *Proteomics* **2015**, *15* (2−3), 260−71.
(20) Li, A.; Zhang, T.; Zheng, M.; Liu, Y.; Chen, Z. Exosomal proteins as potential markers of tumor diagnosis. *J. Hematol. Oncol.* **2017**, *10* (1), 175.
(21) Choi, D. S.; Kim, D. K.; Kim, Y. K.; Gho, Y. S. Proteomics, transcriptomics and lipidomics of exosomes and ectosomes. *Proteomics* **2013**, *13* (10−11), 1554−71.
(22) Balaj, L.; Lessard, R.; Dai, L.; Cho, Y. J.; Pomeroy, S. L.; Breakefield, X. O.; Skog, J. Tumour microvesicles contain retrotransposon elements and amplified oncogene sequences. *Nat. Commun.* **2011**, *2*, 180.
(23) Kahlert, C.; Melo, S. A.; Protopopov, A.; Tang, J.; Seth, S.; Koch, M.; Zhang, J.; Weitz, J.; Chin, L.; Futreal, A.; Kalluri, R. Identification of double-stranded genomic DNA spanning all chromosomes with mutated KRAS and p53 DNA in the serum exosomes of patients with pancreatic cancer. *J. Biol. Chem.* **2014**, *289* (7), 3869−75.
(24) Guescini, M.; Genedani, S.; Stocchi, V.; Agnati, L. F. Astrocytes and Glioblastoma cells release exosomes carrying mtDNA. *J. Neural Transm (Vienna)* **2010**, *117* (1), 1−4.
(25) Valadi, H.; Ekstrom, K.; Bossios, A.; Sjostrand, M.; Lee, J. J.; Lotvall, J. O. Exosome-mediated transfer of mRNAs and microRNAs is a novel mechanism of genetic exchange between cells. *Nat. Cell Biol.* **2007**, *9* (6), 654−9.
(26) Zhao, X.; Wu, Y.; Duan, J.; Ma, Y.; Shen, Z.; Wei, L.; Cui, X.; Zhang, J.; Xie, Y.; Liu, J. Quantitative proteomic analysis of exosome protein content changes induced by hepatitis B virus in Huh-7 cells using SILAC labeling and LC-MS/MS. *J. Proteome Res.* **2014**, *13* (12), 5391−402.
(27) Park, J. E.; Tan, H. S.; Datta, A.; Lai, R. C.; Zhang, H.; Meng, W.; Lim, S. K.; Sze, S. K. Hypoxic tumor cell modulates its microenvironment to enhance angiogenic and metastatic potential by secretion of proteins and exosomes. *Mol. Cell. Proteomics* **2010**, *9* (6), 1085−99.
(28) He, M.; Qin, H.; Poon, T. C.; Sze, S. C.; Ding, X.; Co, N. N.; Ngai, S. M.; Chan, T. F.; Wong, N. Hepatocellular carcinoma-derived exosomes promote motility of immortalized hepatocyte through transfer of oncogenic proteins and RNAs. *Carcinogenesis* **2015**, *36* (9), 1008−18.
(29) www.exocarta.org.
(30) Gonzalez-Begne, M.; Lu, B.; Han, X.; Hagen, F. K.; Hand, A. R.; Melvin, J. E.; Yates, J. R. Proteomic analysis of human parotid gland exosomes by multidimensional protein identification technology (MudPIT). *J. Proteome Res.* **2009**, *8* (3), 1304−14.
(31) Demory Beckler, M.; Higginbotham, J. N.; Franklin, J. L.; Ham, A. J.; Halvey, P. J.; Imasuen, I. E.; Whitwell, C.; Li, M.; Liebler, D. C.; Coffey, R. J. Proteomic analysis of exosomes from mutant KRAS colon cancer cells identifies intercellular transfer of mutant KRAS. *Mol. Cell. Proteomics* **2013**, *12* (2), 343−55.
(32) Steigedal, T. S.; Toraskar, J.; Redvers, R. P.; Valla, M.; Magnussen, S. N.; Bofin, A. M.; Opdahl, S.; Lundgren, S.; Eckhardt, B. L.; Lamar, J. M.; Doherty, J.; Hynes, R. O.; Anderson, R. L.; Svineng, G. Nephronectin is Correlated with Poor Prognosis in Breast Cancer and Promotes Metastasis via its Integrin-Binding Motifs. *Neoplasia* **2018**, *20* (4), 387−400.
(33) Gangoda, L.; Liem, M.; Ang, C. S.; Keerthikumar, S.; Adda, C. G.; Parker, B. S.; Mathivanan, S. Proteomic Profiling of Exosomes Secreted by Breast Cancer Cells with Varying Metastatic Potential. *Proteomics* **2017**, *17* (23-24), 1600370.
(34) Maia, J.; Caja, S.; Strano Moraes, M. C.; Couto, N.; Costa-Silva, B. Exosome-Based Cell-Cell Communication in the Tumor Microenvironment. *Front. Cell Dev. Biol.* **2018**, *6*, 18.
(35) King, H. W.; Michael, M. Z.; Gleadle, J. M. Hypoxic enhancement of exosome release by breast cancer cells. *BMC Cancer* **2012**, *12*, 421.
(36) Green, T. M.; Alpaugh, M. L.; Barsky, S. H.; Rappa, G.; Lorico, A. Breast Cancer-Derived Extracellular Vesicles: Characterization and Contribution to the Metastatic Phenotype. *BioMed Res. Int.* **2015**, *2015*, 634865.
(37) Hoshino, A.; Costa-Silva, B.; Shen, T. L.; Rodrigues, G.; Hashimoto, A.; Tesic Mark, M.; Molina, H.; Kohsaka, S.; Di Giannatale, A.; Ceder, S.; Singh, S.; Williams, C.; Soplop, N.; Uryu, K.; Pharmer, L.; King, T.; Bojmar, L.; Davies, A. E.; Ararso, Y.; Zhang, T.; Zhang, H.; Hernandez, J.; Weiss, J. M.; Dumont-Cole, V. D.; Kramer, K.; Wexler, L. H.; Narendran, A.; Schwartz, G. K.; Healey, J. H.; Sandstrom, P.; Labori, K. J.; Kure, E. H.; Grandgenett, P. M.; Hollingsworth, M. A.; de Sousa, M.; Kaur, S.; Jain, M.; Mallya, K.; Batra, S. K.; Jarnagin, W. R.; Brady, M. S.; Fodstad, O.; Muller, V.; Pantel, K.; Minn, A. J.; Bissell, M. J.; Garcia, B. A.; Kang, Y.; Rajasekhar, V. K.; Ghajar, C. M.; Matei, I.; Peinado, H.; Bromberg, J.; Lyden, D. Tumour exosome integrins determine organotropic metastasis. *Nature* **2015**, *527* (7578), 329−35.
(38) Lowry, M. C.; Gallagher, W. M.; O'Driscoll, L. The Role of Exosomes in Breast Cancer. *Clin. Chem.* **2015**, *61* (12), 1457−65.
(39) Peinado, H.; Aleckovic, M.; Lavotshkin, S.; Matei, I.; Costa-Silva, B.; Moreno-Bueno, G.; Hergueta-Redondo, M.; Williams, C.; Garcia-Santos, G.; Ghajar, C.; Nitadori-Hoshino, A.; Hoffman, C.; Badal, K.; Garcia, B. A.; Callahan, M. K.; Yuan, J.; Martins, V. R.; Skog, J.; Kaplan,


DOI: 10.1021/acs.jproteome.8b00859
*J. Proteome Res.* 2019, 18, 1237−1247

R. N.; Brady, M. S.; Wolchok, J. D.; Chapman, P. B.; Kang, Y.; Bromberg, J.; Lyden, D. Melanoma exosomes educate bone marrow progenitor cells toward a pro-metastatic phenotype through MET. *Nat. Med.* **2012**, *18* (6), 883−91.
(40) Ochieng, J.; Pratap, S.; Khatua, A. K.; Sakwe, A. M. Anchorage-independent growth of breast carcinoma cells is mediated by serum exosomes. *Exp. Cell Res.* **2009**, *315* (11), 1875−88.
(41) Shevchenko, A.; Wilm, M.; Vorm, O.; Mann, M. Mass spectrometric sequencing of proteins silver-stained polyacrylamide gels. *Anal. Chem.* **1996**, *68* (5), 850−8.
(42) Rappsilber, J.; Ishihama, Y.; Mann, M. Stop and go extraction tips for matrix-assisted laser desorption/ionization, nanoelectrospray, and LC/MS sample pretreatment in proteomics. *Anal. Chem.* **2003**, *75* (3), 663−70.
(43) Cox, J.; Mann, M. MaxQuant enables high peptide identification rates, individualized p.p.b.-range mass accuracies and proteome-wide protein quantification. *Nat. Biotechnol.* **2008**, *26* (12), 1367−72.
(44) Cox, J.; Hein, M. Y.; Luber, C. A.; Paron, I.; Nagaraj, N.; Mann, M. Accurate proteome-wide label-free quantification by delayed normalization and maximal peptide ratio extraction, termed MaxLFQ. *Mol. Cell. Proteomics* **2014**, *13* (9), 2513−26.
(45) https://github.com/JurgenCox/perseus-plugins.
(46) Tusher, V. G.; Tibshirani, R.; Chu, G. Significance analysis of microarrays applied to the ionizing radiation response. *Proc. Natl. Acad. Sci. U. S. A.* **2001**, *98* (9), 5116−21.
(47) Ingenuity Pathway Analysis. https://www.qiagenbioinformatics.com/products/ingenuity-pathway-analysis/.
(48) Wu, Y.; Deng, W.; Klinke, D. J., 2nd Exosomes: improved methods to characterize their morphology, RNA content, and surface protein biomarkers. *Analyst* **2015**, *140* (19), 6631−42.
(49) Xu, K.; Liu, P.; Wei, W. mTOR signaling in tumorigenesis. *Biochim. Biophys. Acta, Rev. Cancer* **2014**, *1846* (2), 638−54.
(50) Yan, J.; Zhang, B.; Hosseinzadeh, Z.; Lang, F. Down-Regulation of Store-Operated Ca2+ Entry and Na+ Ca2+ Exchange in MCF-7 Breast Cancer Cells by Pharmacological JAK3 Inhibition. *Cell. Physiol. Biochem.* **2016**, *38* (4), 1643−51.
(51) Vaidya, S. M.; Kamalakar, P. L. Copper and ceruloplasmin levels in serum of women with breast cancer. *Indian J. Med. Sci.* **1998**, *52* (5), 184−7.
(52) Brandenberger, R.; Schmidt, A.; Linton, J.; Wang, D.; Backus, C.; Denda, S.; Müller, U.; Reichardt, L. F. Identification and characterization of a novel extracellular matrix protein nephronectin that is associated with integrin $\alpha 8\beta 1$ in the embryonic kidney. *J. Cell Biol.* **2001**, *154* (2), 447−458.
(53) Amorim, M.; Fernandes, G.; Oliveira, P.; Martins-de-Souza, D.; Dias-Neto, E.; Nunes, D. The overexpression of a single oncogene (ERBB2/HER2) alters the proteomic landscape of extracellular vesicles. *Proteomics* **2014**, *14* (12), 1472−9.
(54) Nazarenko, I.; Rana, S.; Baumann, A.; McAlear, J.; Hellwig, A.; Trendelenburg, M.; Lochnit, G.; Preissner, K. T.; Zoller, M. Cell surface tetraspanin Tspan8 contributes to molecular pathways of exosome-induced endothelial cell activation. *Cancer Res.* **2010**, *70* (4), 1668−78.
(55) Thompson, C. A.; Purushothaman, A.; Ramani, V. C.; Vlodavsky, I.; Sanderson, R. D. Heparanase regulates secretion, composition, and function of tumor cell-derived exosomes. *J. Biol. Chem.* **2013**, *288* (14), 10093−9.
(56) Kahai, S.; Lee, S. C.; Lee, D. Y.; Yang, J.; Li, M.; Wang, C. H.; Jiang, Z.; Zhang, Y.; Peng, C.; Yang, B. B. MicroRNA miR-378 regulates nephronectin expression modulating osteoblast differentiation by targeting GalNT-7. *PLoS One* **2009**, *4* (10), e7535.
(57) Munkley, J.; Elliott, D. J. Hallmarks of glycosylation in cancer. *Oncotarget* **2016**, *7* (23), 35478−89.
(58) Pinho, S. S.; Reis, C. A. Glycosylation in cancer: mechanisms and clinical implications. *Nat. Rev. Cancer* **2015**, *15* (9), 540−55.
(59) Menck, K.; Scharf, C.; Bleckmann, A.; Dyck, L.; Rost, U.; Wenzel, D.; Dhople, V. M.; Siam, L.; Pukrop, T.; Binder, C.; Klemm, F. Tumor-derived microvesicles mediate human breast cancer invasion through differentially glycosylated EMMPRIN. *J. Mol. Cell Biol.* **2015**, *7* (2), 143−53.
(60) Moreno-Gonzalo, O.; Villarroya-Beltri, C.; Sanchez-Madrid, F. Post-translational modifications of exosomal proteins. *Front. Immunol.* **2014**, *5*, 383.
(61) Liang, Y.; Eng, W. S.; Colquhoun, D. R.; Dinglasan, R. R.; Graham, D. R.; Mahal, L. K. Complex N-linked glycans serve as a determinant for exosome/microvesicle cargo recruitment. *J. Biol. Chem.* **2014**, *289* (47), 32526−37.
(62) Schwarz, F.; Aebi, M. Mechanisms and principles of N-linked protein glycosylation. *Curr. Opin. Struct. Biol.* **2011**, *21* (5), 576−82.
(63) Gill, D. J.; Chia, J.; Senewiratne, J.; Bard, F. Regulation of O-glycosylation through Golgi-to-ER relocation of initiation enzymes. *J. Cell Biol.* **2010**, *189* (5), 843−58.
(64) Goldenring, J. R. A central role for vesicle trafficking in epithelial neoplasia: intracellular highways to carcinogenesis. *Nat. Rev. Cancer* **2013**, *13* (11), 813−20.
(65) Mauvezin, C.; Neufeld, T. P. Bafilomycin A1 disrupts autophagic flux by inhibiting both V-ATPase-dependent acidification and Ca-P60A/SERCA-dependent autophagosome-lysosome fusion. *Autophagy* **2015**, *11* (8), 1437−8.
(66) Cauwe, B.; Opdenakker, G. Intracellular substrate cleavage: a novel dimension in the biochemistry, biology and pathology of matrix metalloproteinases. *Crit. Rev. Biochem. Mol. Biol.* **2010**, *45* (5), 351−423.
(67) Shiomi, T.; Lemaitre, V.; D'Armiento, J.; Okada, Y. Matrix metalloproteinases, a disintegrin and metalloproteinases, and a disintegrin and metalloproteinases with thrombospondin motifs in non-neoplastic diseases. *Pathol. Int.* **2010**, *60* (7), 477−96.
(68) Shimoda, M.; Khokha, R. Proteolytic factors in exosomes. *Proteomics* **2013**, *13* (10−11), 1624−36.
(69) Roucourt, B.; Meeussen, S.; Bao, J.; Zimmermann, P.; David, G. Heparanase activates the syndecan-syntenin-ALIX exosome pathway. *Cell Res.* **2015**, *25* (4), 412−28.
(70) Vizcaino, J. A.; Csordas, A.; del-Toro, N.; Dianes, J. A.; Griss, J.; Lavidas, I.; Mayer, G.; Perez-Riverol, Y.; Reisinger, F.; Ternent, T.; Xu, Q. W.; Wang, R.; Hermjakob, H. 2016 update of the PRIDE database and its related tools. *Nucleic Acids Res.* **2016**, *44* (D1), D447−56.
(71) PRIDE. https://www.ebi.ac.uk/pride/archive/projects/PXD010999.


DOI: 10.1021/acs.jproteome.8b00859
*J. Proteome Res.* 2019, 18, 1237−1247